NeuroImage 000 (2021) 118614

Contents lists available at ScienceDirect

NeuroImage

journal homepage: www.elsevier.com/locate/neuroimage

Identifying brain regions supporting amygdalar functionality: Application of a novel graph theory technique

Melanie A. Matyi[a,*], Sebastian M. Cioaba[b], Marie T. Banich[c], Jeffrey M. Spielberg[a]

[a] Department of Psychological and Brain Sciences, University of Delaware, Newark, DE 19716, USA
[b] Department of Mathematical Sciences, University of Delaware, Newark, DE 19716, USA
[c] Department of Psychology and Neuroscience, University of Colorado Boulder, Boulder, CO 80309, USA

ARTICLE INFO

Keywords:
Amygdala
Graph theory
Brain network

ABSTRACT

Effective amygdalar functionality depends on the concerted activity of a complex network of regions. Thus, the role of the amygdala cannot be fully understood without identifying the set of brain structures that allow the processes performed by the amygdala to emerge. However, this identification has yet to occur, hampering our ability to understand both normative and pathological processes that rely on the amygdala. We developed and applied novel graph theory methods to diffusion-based anatomical networks in a large sample ($n = 1{,}052$, 54.28% female, mean age=28.75) to identify nodes that critically support amygdalar interactions with the larger brain network. We examined three graph properties, each indexing a different emergent aspect of amygdalar network communication: *current-flow betweenness centrality* (amygdalar influence on information flowing between other pairs of nodes), *node communicability* (clarity of communication between the amygdala and other nodes), and *subgraph centrality* (amygdalar influence over local network processing). Findings demonstrate that each of these aspects of amygdalar communication is associated with separable sets of regions and, in some cases, these sets map onto previously identified sub-circuits. For example, *betweenness* and *communicability* were each associated with different sub-circuits that have been identified in previous work as supporting distinct aspects of memory-guided behavior. Other regions identified span basic (e.g., visual cortex) to higher-order (e.g., insula) sensory processing and executive functions (e.g., dorsolateral prefrontal cortex). Present findings expand our current understanding of amygdalar function by showing that there is no single 'amygdala network', but rather multiple networks, each supporting different modes of amygdalar interaction with the larger brain network. Additionally, our novel method allowed for the identification of *how* such regions support the amygdala, which has not been previously explored.

The amygdala is critically involved in a variety of complex emotional and motivational processes (Cardinal et al., 2002; Lang and Davis, 2006), and amygdalar processing is disturbed across a range of psychological disorders (Evans et al., 2008; He et al., 2019; Zhang et al., 2020). Decades of research have resulted in the identification of regions that show complex interactions with amygdala (Phelps et al., 2004), and these regions likely support the capacity for amygdala to efficiently and effectively interact with the larger brain network. However, past work has been unable to provide insight into *the manner in which* such regions support amygdalar functionality. Specifically, the way in which the amygdala interacts with the larger network depends on a number of factors, including the extent to which signals pass through (and thus can be influenced by) the amygdala on their way to other areas, the quality (i.e., signal-to-noise) of amygdalar communication, and the extent to which amygdala is able to influence communication specifically within sub-networks. Although past work has identified regions that interact with amygdala, it has not specified which of these factors, if any, are supported by a given region. In fact, it is entirely possible that separate sets of brain regions support these different factors.

Unfortunately, extant methods in humans cannot provide insight into the factors that modulate amygdala communication, and thus a novel approach is needed to address this key gap in the literature. Specifically, past work has largely employed a 'bivariate' perspective – examining the link between a pair of regions (i.e., the amygdala and a region with which it is connected) – while ignoring the placement of that link within the context of the larger network that constitutes the brain. For example, visual information arrives at the amygdala via multiple routes (Pessoa and Adolphs, 2010). Thus, removal of one route will not prevent this information from being delivered to the amygdala, a fact that is not evident when only a single connection is examined. In order to parse the

* Corresponding author.
E-mail address: mmatyi@udel.edu (M.A. Matyi).

https://doi.org/10.1016/j.neuroimage.2021.118614.
Received 23 April 2021; Accepted 21 September 2021
Available online xxx.

different factors mentioned above, it is necessary to examine how the particular *arrangement* of (direct and indirect) amygdalar connections facilitates or impedes amygdalar communication within the broader brain network. This can be done by leveraging graph theory methods that index emergent properties of brain regions (Rubinov and Sporns, 2010). There are a number of ways in which the amygdala could influence processing in other brain regions, each of which can be indexed via different graph theory metrics. For example, the amygdala could serve as a *bottleneck* through which information from one area of the network must flow to reach other areas. Such 'hub' nodes are critical to integrating distributed information, and it is the *position* of a node within the network that confers 'hubness' rather than the number/strength of the node's connections *per se*. As described below, this role can be indexed via *current-flow (CF) betweenness centrality*. A second way that the amygdala could influence processing in other brain regions is if it sends information to a given region via *multiple (parallel) paths*, because this will reduce the impact of noise added along each individual pathway. As described below, this role can be indexed via *node communicability*. These two 'network properties', as we will refer to them, focus on amygdalar influence on processing across the entire network, but of equal importance is amygdalar influence within its local network (i.e., nodes that it is strongly connected to, either directly or indirectly). In particular, one of the fundamental organizing principles of networks is *segregation*, in which the presence of clusters of highly connected nodes (i.e., local networks) allows for specialized processing to occur within the different network clusters (Sporns, 2013). The amygdala will influence processing in its local network if it has multiple 'self-loops' (paths that start and end at the amygdala), because such loops allow for recursive processing that reincorporates amygdala-related information. As described below, this role can be indexed via *subgraph centrality*.

The network properties introduced above are not competing, but rather describe different aspects of how amygdalar interaction/influence can occur. Although typical graph methods allow for the identification of *how much* a node influences the network, they do not reveal the *network that supports this influence*. Identifying the regions that support each amygdalar network property is crucial for understanding the precise neural mechanisms that result in amygdala-related psychological processes, along with the manner in which such processes go awry in pathology.

The present study proposes and applies a novel graph theory technique for identifying which region(s) support different factors that facilitate amygdalar influence within the brain. Graph methods have been used previously to assess the impact of a region on global processes via 'virtual lesioning' (Alstott et al., 2009; Owen et al., 2016; Pestilli et al., 2014; Schmitt et al., 2012; Stam, 2014). 'Virtual lesioning' methods 'remove' (e.g., set its links to zero or remove it entirely from the connectivity matrix) a node from the network and examine the impact of this removal on a property of the entire brain network. For example, past work has examined overall network robustness by (i) computing global network properties (e.g., overall communication efficiency) on the full network, (ii) excluding a node (a 'virtual lesion') and re-computing global properties on the reduced network, and (iii) comparing the values from the reduced network against those from the full network to determine how easily global processes can be disturbed (Kaiser et al., 2007). This approach is valuable for providing information about the extent to which individual brain regions support emergent processes in the *overall* network, but it does not allow for examination of how one region supports the emergent network properties of another region (e.g., amygdala), which is the goal of the present work.

1. Novel 'virtual lesion' method

In the present study we developed a novel extension of the 'virtual lesioning' methodology (described in detail below) and applied it to structural brain networks (derived from diffusion-weighted imaging) to elucidate the architecture needed to support effective amygdalar interactions within the larger network. Specifically, we examined how the exclusion of a (non-amygdala) network node impacts network properties of the amygdala, rather than how the removal of a given node influences properties of the global network, as done in previous 'lesioning' techniques. That is, instead of looking at the impact that a single node has on the network as a whole (e.g., Alstott et al., 2009), we examined the impact of single nodes on the ability of the amygdala to effectively operate within the network. Consequently, 'virtual lesioning' techniques used in past work can provide information about the role of the 'lesioned' region in the global network, whereas our technique provides information about the contribution of (non-amygdala) regions to amygdalar communication in the network. Furthermore, by examining multiple types of network properties, our method allows us to identify *which nodes* support *which aspects* of amygdalar communication.

For clarity, we will refer to the amygdala as the 'focal' node and all other regions as 'satellite' nodes. As illustrated in Fig. 1, our 'virtual lesion' method entails (i) calculating measures of amygdalar centrality (i.e., graph theory properties that assay an aspect of how the amygdala interacts within the brain network) in the full network, (ii) iteratively excluding each satellite node from the network and recalculating amygdalar centrality after each exclusion, and (iii) comparing amygdalar centrality with and without each satellite node. In other words, for each satellite node, we computed the difference between amygdala centrality in the full network (i.e., no nodes removed) and in the 'reduced' network (i.e., with the current satellite node removed). This difference indexes the extent to which that specific satellite node supports a particular mode of amygdala interaction with the network (i.e., amygdalar centrality in the brain). To be clear, only one satellite node is excluded at a time to create the 'reduced' network.

In summary, this method identifies nodes that, when 'lesioned', decrease the centrality of the amygdala, thereby identifying the network of satellite nodes crucial to supporting each amygdalar network property. Importantly, the method applied here is an extension of that used in previous studies, and thus the basic 'virtual lesioning' framework (i.e., removing a node and examining the impact of this removal on graph metrics) has been validated in a number of past studies (Alstott et al., 2009; Kaiser et al., 2007; Owen et al., 2016; Schmitt et al., 2012). We extended this basic framework by focusing on graph metrics that are node-specific (i.e., indexing an aspect of a particular node) rather than global (i.e., indexing an aspect of the entire network).

We focused on graph metrics assaying amygdalar centrality, as these metrics capture different types of influence that the amygdala has on other regions in the network. In particular, we chose the three complementary metrics mentioned above. *Current-flow (CF) betweenness centrality* (Brandes and Fleischer, 2005; Newman, 2005) is the amount of network flow that goes *through* a node, thus indexing the extent to which the amygdala *influences information flow between* all pairs of nodes in the network (i.e., functions as a communication hub/bottleneck). *Node communicability* (Benzi and Klymko, 2013; Estrada and Hatano, 2008) reflects the number of different, parallel paths that information can travel between the amygdala and each node in the rest of the brain. Thus, this property indexes the extent to which the amygdala can transmit information 'clearly' with all nodes in the network, because information traveling along multiple paths will (on average) increase the amount of 'signal' from the amygdala relative to 'noise' from the network. *Subgraph centrality* (Estrada and Rodriguez-Velazquez, 2005) reflects the number of random paths that start from a given node and traverse back to that node (i.e., self-loops). Given that these loops allow for recursive processing that reincorporates amygdala-related information, this property indexes the extent to which the amygdala influences local networks. The criteria used to choose metrics are described more fully in the Methods section.

In order to depict how our 'lesioning' procedure operates on each centrality metric, we provide examples using 'toy' networks (Figs. 2–4). In particular, these figures illustrate how the removal of a satellite node (labeled with an 'S') impacts each type of centrality for the focal node

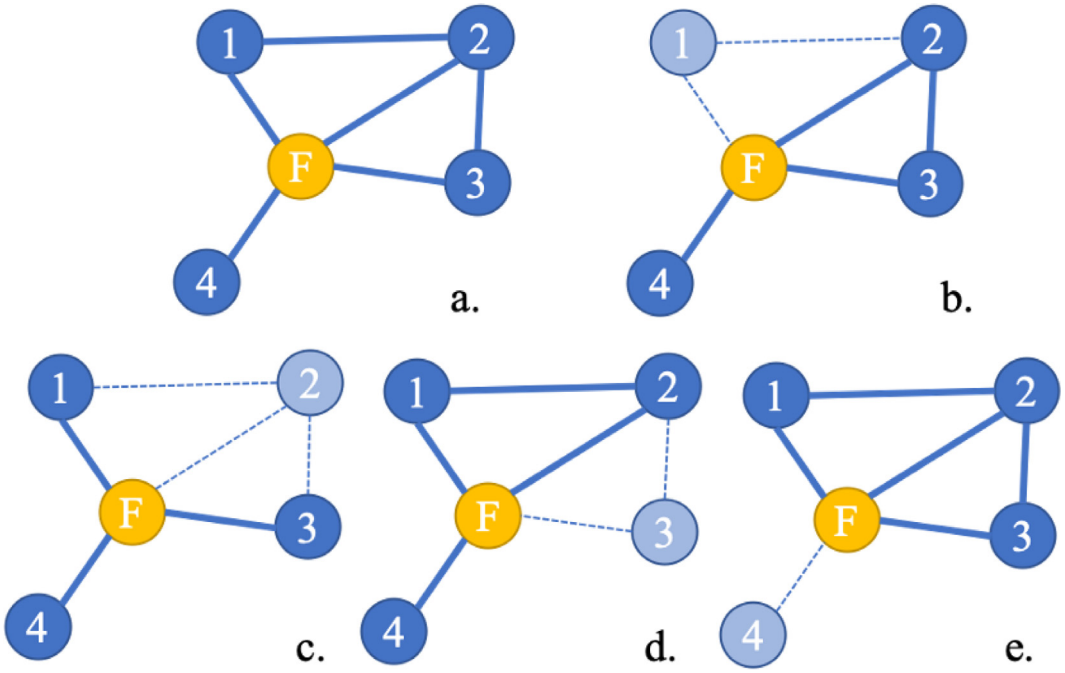

Fig. 1. Illustration of virtual lesion method.
Yellow nodes represent focal node of interest. Dark blue nodes represent satellite nodes included in calculation of centrality measures. Light blue nodes represent removed ('virtually lesioned') satellite nodes not included in recalculation of centrality measures. Panel A shows a 'full' network (all nodes included), whereas panels B-E show 'reduced' networks (one satellite node removed). Centrality is first calculated for the focal node in the full network (A) and then recalculated (for the focal node) following the removal of satellite node 1 (B), node 2 (C), node 3 (D), and node 4 (E). Change in focal node centrality is calculated for each removed node by subtracting the centrality value of the focal node in the full network (A) from each reduced network (B–E).

(labeled with an 'F') of interest (i.e., amygdala). Detailed descriptions for each metric are provided in the figure legends.

We examined diffusion-based structural (as opposed to functional) brain networks, because a 'connection' between two nodes in a functional network (correlated activity between two nodes) reflects sources other than those nodes, including the influence of a third node that connects to both of the nodes. Thus, a 'virtual lesion' cannot completely remove the influence of a node in functional data, as that variance remains present in other connections in the network. This is not true of diffusion-based networks, as they reflect the specific white matter pathways between node pairs, and thus the removal of a node (and the pathways leading to it) removes the influence of that node in the organization of the network. Therefore, the interpretation of 'virtual lesioning' of diffusion networks is significantly clearer than if applied to functional networks. To be clear, we are not arguing that the physical removal (i.e., surgical lesion) of a node would not (eventually) result in changes to pathways connected to other nodes (i.e., reorganization). Rather, 'virtual' removal of a node allows us to see the manner in which it's placement in the network (as it currently stands) influences amygdalar capabilities. Moreover, functional networks are constrained by their structural underpinnings (Horn et al., 2014), and thus, diffusion-based estimates of a network reflect the *capability* of that network to communicate, rather than actual communication. Given that we are interested in identifying regions that support the amygdala's *capability to interact with other brain regions* and the clearer interpretation of "lesioning" diffusion networks, examining diffusion-based networks represents the logical first step.

To identify the sets of satellite (i.e., non-amygdala) nodes that are particularly crucial for each metric, we conducted pairwise comparisons between the metrics (for each satellite node). This approach allowed us to determine whether a satellite node was more important for one metric than the others. To enhance the robustness and reproducibility of the findings, the 1052 participants were randomly grouped into ten sets (105 or 106 participants per set), all statistical analyses were carried out within each set, and only findings that were significant (after within-set correction for multiple comparisons) *across all sets* were retained. This approach leverages the large sample size in such a way as to maximize the robustness and replicability of the present findings.

2. Materials and methods

2.1. Participant data

We used data collected from 1053 healthy participants [*M* age = 28.75, SD = 3.68; female = 571 (54.28%); White = 798 (75.86%), Black = 148 (14.06%), Asian/Pacific = 63 (5.98%), American Indian/Alaskan = 2 (0.19%), Multiple = 26 (2.47%), Not reported = 15 (1.43%), Hispanic/Latino = 88 (8.37%)] as part of the Human Connectome Project (HCP). Briefly, the HCP offers a database of anonymous structural, diffusion, and functional MRI for research purposes (Van Essen et al., 2013). We conducted secondary analysis on de-identified open access data after agreeing to the HCP Open Access Data Use Terms. Informed consent, including consent to share de-identified data, was acquired by the HCP and approved by the Washington University institutional review board. One subject was excluded because their structural network became disconnected after calculation of graph theory metrics, leading to a final $n = 1052$.

2.2. Graph metrics

Three properties measuring different aspects of centrality were calculated for each participant, for each hemisphere, for each node. We selected only a small number of metrics for several reasons, including to avoid type 1 error and because of the complex (and thus time consuming) computational requirements of metric computation (on top of probabilistic tracking). As mentioned above, we used several criteria to select from among the wider array of available properties: (i) *We chose graph properties based on frameworks appropriate for brain networks*. Specifically,

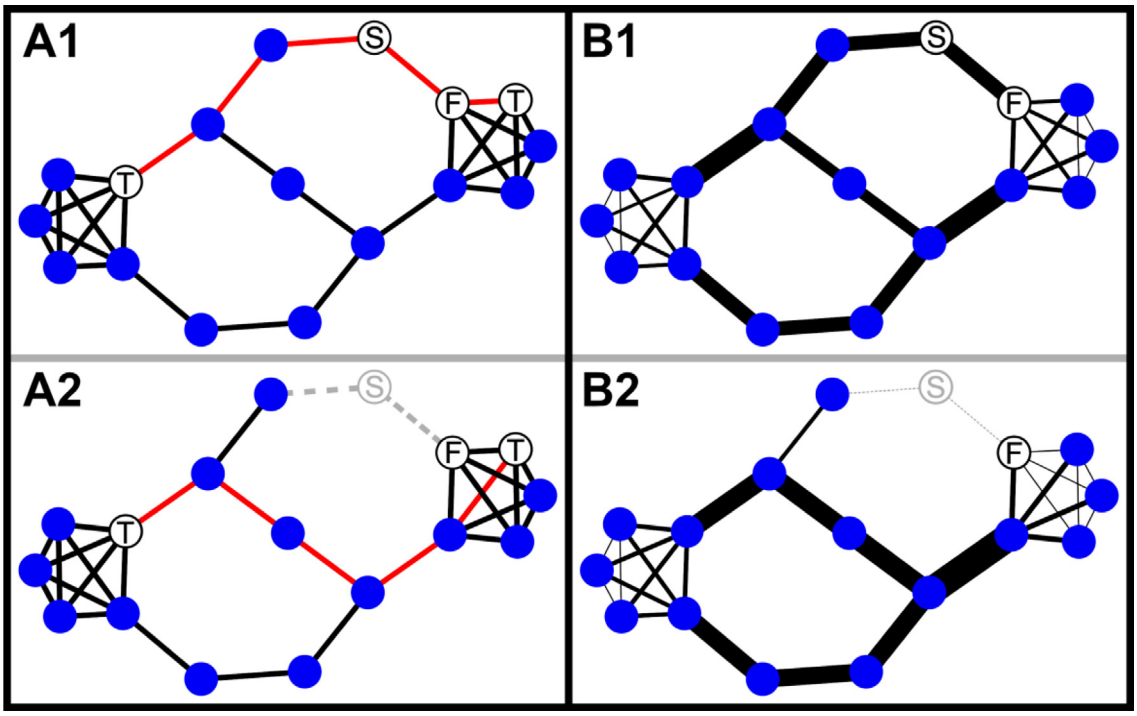

Fig. 2. Toy network demonstration of the novel virtual lesion method on betweenness centrality.
The figure above demonstrates the impact of removing (i.e., 'virtually lesioning') a satellite node (labeled 'S') on the betweenness centrality of the focal node (labeled 'F') of interest (i.e., amygdala). Betweenness centrality reflects the influence that a node has over communication between all pairs of nodes in the network. In other words, a node will have high betweenness if information from one part of the network must flow through that node in order to reach another part of the network. Although the current-flow version of betweenness centrality was used in the present work, the shortest-path version of betweenness provides a conceptually simpler (and thus clearer) demonstration of our method. Therefore, we first demonstrate our method via shortest-path betweenness (Panels A1/A2) and then extend to current-flow betweenness (Panels B1/B2). *Panel A (shortest path framework)*: For ease of demonstration, we focus on the influence of the focal node 'F' only on the communication between two 'target' nodes (labeled 'T'), as presenting communication between all pairs of nodes in the network would be overly complex. In A1 and A2, the red lines represent the shortest path between the two target ('T') nodes. In A1, we see that the shortest path flows through focal node 'F', thus allowing node 'F' to influence the communication between these nodes. In A2, we see that the shortest path no longer flows through the focal node 'F' after the satellite node 'S' has been 'lesioned'. Thus, satellite node 'S' appears to support the betweenness centrality of focal node 'F'. *Panel B (current-flow framework)*: In both B1 and B2, the width of the black lines represents the amount of communication flowing through each connection (in this case taking into account communication between all pairs of nodes, which is why no 'target' nodes are present). In B1, we see that a relatively large amount of information will flow into focal node 'F' (as indicated by the thick connection between nodes 'S' and 'F'), allowing node 'F' to influence this communication. In B2, we see that removal of satellite node 'S' significantly decreases the amount of information flowing though focal node 'F' (i.e., by 1.8 standard deviations). Note, the network above is the same as network 2 in Fig. 3 of Newman (2005), the original presentation of Current-Flow Betweenness Centrality.

all graph properties rest on assumptions about the underlying network, and several common properties rest on assumptions which are violated with brain networks (Fornito et al., 2016). For example, properties that depend on the 'shortest paths' are not appropriate (Goñi et al., 2013), given that they assume that only the shortest path is used/relevant. The shortest path framework would be appropriate in a transportation network, where a vehicle travels only one route. However, brain networks function via parallel transfer (i.e., one neuron can excite multiple neurons; Fornito et al., 2016), and thus it is necessary to take multiple paths into account, which a shortest path framework does not do. In contrast, properties based on either a current flow (CF) model or the matrix exponential (i.e., communicability) are appropriate for the mechanisms by which information flows in brain networks, because they incorporate the influence of all potential paths, weighting this influence by path length (i.e., longer paths are down-weighted). Thus, these properties reflect the fact that shorter, more direct paths between regions are likely more important to communication between brain regions than longer, more indirect paths. (ii) *We chose properties that are theoretically relevant for brain processing.* Specifically, we selected properties that index the influence of a node over processing in the local and global network and the quality of this communication, given that these were the specific aspects of network communication that were of interest. (iii) *We selected graph properties in which removing a node provides an interpretable and interesting impact on the metric*. For example, removing node *X* would have an interpretable impact on amygdalar node strength (i.e., sum of the links attached to a node), but this impact would be uninteresting as it would simply reflect the weight of the link connecting amygdala to node *X*. Conversely, although the impact of removing a node on amygdalar clustering coefficient could potentially be interesting, this impact is much less amenable to a clear interpretation. Additionally, we selected properties that incorporate both direct and indirect connections. In particular, many properties are based solely, or principally, on first-order connectivity (i.e., direct connections to a node), which would not allow us to identify nodes that play a crucial supportive role for amygdala but are not directly connected.

Thus, we examined one current-flow-based measure (CF betweenness centrality) and two communicability-based measures (node communicability and subgraph centrality). All of these metrics are (i) based on appropriate frameworks, (ii) are theoretically relevant for brain processing, and (iii) have an interpretable and interesting impact. *CF betweenness* measures the extent to which a node influences information flow between other nodes (Brandes and Fleischer, 2005; Newman, 2005). *Node communicability* measures the extent to which a node can transmit information clearly with each other node (Benzi and Klymko, 2013; Estrada and Hatano, 2008). *Subgraph centrality* measures the extent to which a node influences communication in local networks

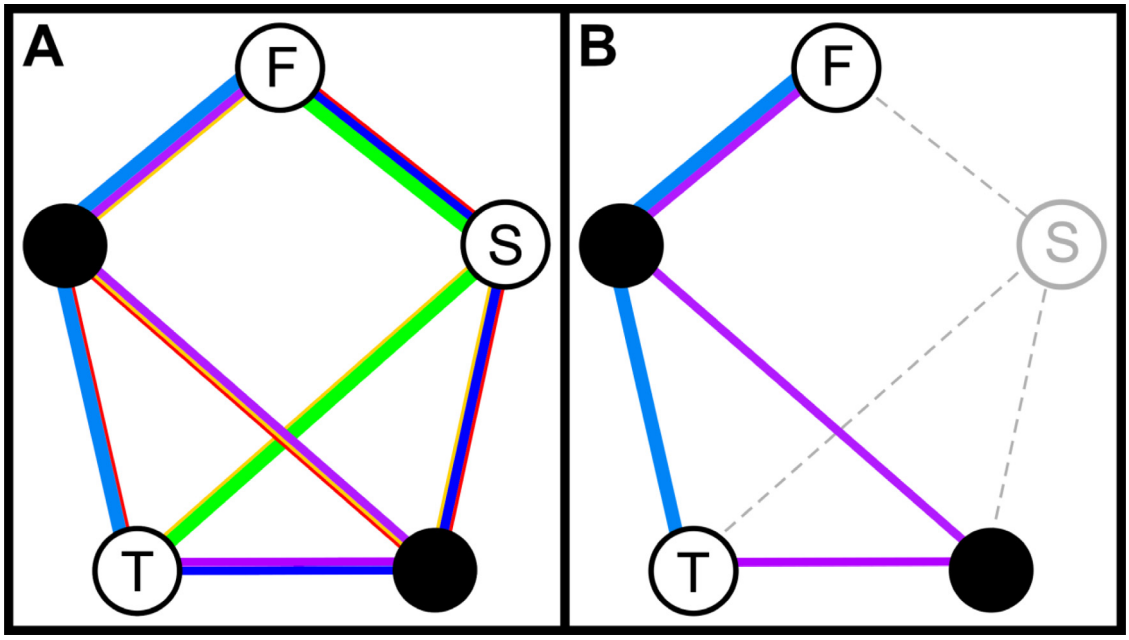

Fig. 3. Toy network demonstration of the novel virtual lesion method on node communicability. (For interpretation of the references to color in this figure, the reader is referred to the web version of this article).
The figure above demonstrates the impact of removing (i.e., 'virtually lesioning') a satellite node (labeled 'S') on the node communicability of the focal node (labeled 'F') of interest (i.e., amygdala). Node communicability indexes a node's ability to send/receive information clearly (i.e., without interference) to/from other parts of the network. Specifically, transmission of information between two nodes will be clearer (i.e., less degradation from noise) when there is a higher number of parallel paths between the nodes for information to travel along. Communicability reflects the clarity of communication between one node and a 'target' node, and *node* communicability is the sum of all the communicabilities associated with a single node (i.e., average clarity of communication between one node and the rest of the network). The networks above reflect communicability between the focal node and only a single 'target' node (labeled 'T'), which was done for ease of illustration, as presenting the communicabilities between node 'F' and all other nodes would be overly complex. In our novel method, the satellite node 'S' is removed to quantify the extent to which the 'S' node supports the communicability of the 'F' node. Panel A above reflects the full network, and Panel B reflects that 'lesioned' network. Each line color in the panels above represents one of the possible paths between the focal node 'F' and the target node 'T', and the thickness of the lines reflects the length of that path. For example, the two thick light blue lines represent one path between the two nodes, and the lines are thick, because this is a short (two-hop) path. The four red lines in panel A represent another path between the two nodes, and these lines are thin, because this is a long (four-hop) path. In panel A, we see that there are six possible paths between the two nodes, allowing for significant parallel (and thus clearer) communication. In panel B, we see that the removal of the satellite node 'S' decreases the possible number of paths between the focal node 'F' and the target node 'T' to two, thus decreasing the potential clarity of communication between these nodes. Overall, the removal of satellite node 'S' reduces the *node* communicability of focal node 'F' by 2 standard deviations.

(Estrada and Rodriguez-Velazquez, 2005). See Supplementary Material for the formulas used to compute each centrality measure and discussion of the normalization factors used in the calculation of *node communicability* and *subgraph centrality*.

2.3. Data acquisition

Structural and diffusion-weighted data were acquired on a modified 3T Skyra System (Siemens) using a 32-channel coil. A T1-weighted structural image was acquired (TR = 2400 ms; TE = 2.14 ms; TI = 1000 ms; flip angle = 8°; voxel size = .7 x. 7 x. 7 mm; Uğurbil et al., 2013). Diffusion acquisition involved a spin-echo EPI sequence (Feinberg et al., 2010; Setsompop et al., 2012) with multiband EPI (Moeller et al., 2010; Junqian Xu et al., 2012) and 270 diffusion-weighted directions (TR = 5520 ms; TE = 89.5 ms; flip angle = 78°; refocusing flip angle = 160°; voxel size = 1.25 × 1.25 × 1.25 mm; multiband factor = 3; b-values = 1000, 2000, 3000 s/mm^2; Sotiropoulos et al., 2013; Uğurbil et al., 2013).

2.4. HCP MRI preprocessing

All imaging data passed HCP quality assurance (Marcus et al., 2013) and were run (by HCP) through several standardized preprocessing pipelines. The use of this (standardized) preprocessed data allows for greater methodological transparency and replicability across studies. Structural T1-weighted images first underwent gradient distortion and bias field correction. Next, T1 images were run through FreeSurfer to obtain a participant-specific subcortical segmentation, delineation of the cortical mantle, and segmentation of a white matter mask (Fischl, 2012). Diffusion data were run through an HCP pipeline in FSL to normalize b_0 image intensity across runs, and to correct for EPI distortion, eddy-current induced distortions, gradient-nonlinearities, and subject motion (Glasser et al., 2013; Jenkinson et al., 2012). Next, diffusion data was analyzed with FSL's bedpostx toolbox which creates the files necessary for performing probabilistic tractography (Hernandez-Fernandez et al., 2019).

2.5. Connectivity atlas

We used an atlas that included a 182-region (per hemisphere) cortical parcellation created by HCP using multi-modal imaging data (Glasser et al., 2016), in conjunction with a 6-region (per hemisphere) subject-specific subcortical segmentation obtained via FreeSurfer (Fischl et al., 2002). The cortical atlas was warped to each participant's cortical mantle using FreeSurfer transformations, then projected into 3d space. The HCP atlas and FreeSurfer segmentation each generated hippocampus ROIs, which were combined, thus resulting in a total of 186 nodes per hemisphere. Networks were calculated separately for right and left hemispheres, because the relatively few contralateral (vs. ipsilateral) amygdalar connections are known from tracing studies to be light and mimic the much denser ipsilateral

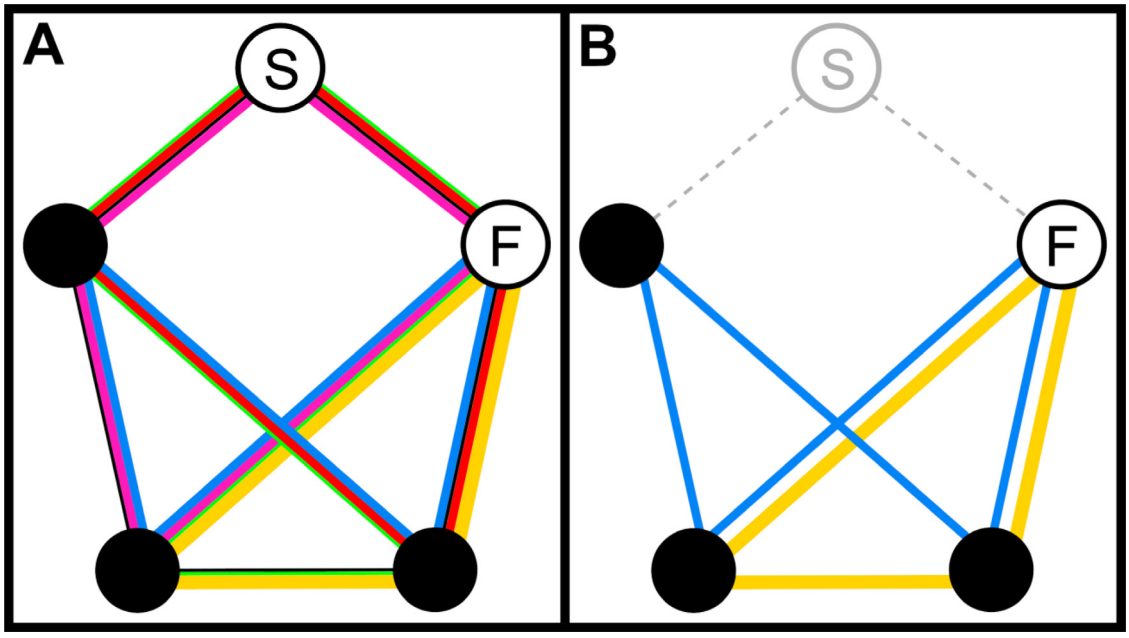

Fig. 4. Toy network demonstration of the novel virtual lesion method on subgraph centrality.
The figure above demonstrates the impact of removing (i.e., 'virtually lesioning') a satellite node (labeled 'S') on the subgraph centrality of the focal node (labeled 'F') of interest (i.e., amygdala). Subgraph centrality indexes the level of influence that a node has over processing in the local network. Specifically, a node will have more influence in the local network when there are a larger number of paths that leave from and return to that node (i.e., closed walks), given that this allows for recursive processing that reincorporates information from the focal node. In our novel method, the satellite node 'S' is 'lesioned' to quantify the extent to which the 'S' node supports the subgraph centrality of the focal node 'F'. Panel A above reflects the full network, and Panel B reflects that 'lesioned' network. Each line color in the panels above represents one of the possible paths that leaves from and returns to the focal node 'F', and the thickness of the lines reflects the length of that path. For example, the three thick yellow lines represent one closed walk, and the lines are thick, because this is a short (three-hop) path. The five green lines in Panel A represent another closed walk, and these lines are thin, because this is a long (five-hop) path. In panel A, we see that there are six total closed walks, which allow the focal node 'F' to exert a high level of influence in this (local) network. In panel B, we see that only two closed walks remain after the satellite node 'S' is removed, significantly decreasing the influence of the focal node 'F' (i.e., decreasing the subgraph centrality of node 'F' by 1.4 standard deviations).

connections (McDonald, 1998). FreeSurfer ROIs representing white matter were combined to create a white matter mask for use in tractography.

2.6. Creation of connectivity matrices

Interregional white matter connectivity was estimated using probabilistic tractography (Behrens et al., 2007; Jbabdi et al., 2012) via FSL's probtrackx2, which infers the orientation of a tract by repeatedly sampling from the principal diffusion direction calculated in bedpostx. A distribution of the tract's path from each voxel using these estimates is then built. Multiple tracts are sampled from each voxel, and each propagation step is based on a randomly chosen orientation from the probability map. The estimated connectivity between two regions is equal to the probability of a tract starting at the seed region and going through the target region (Behrens et al., 2003). To obtain connectivity estimates from each ROI to every other ROI in the atlas, tractography was performed using the GPU version of probtrackx2 with the following options (in addition to the compulsory arguments): 'network' (use network mode, which only retains paths that meet a different seed mask), 'loopcheck' (stop if path loops back on itself), 'opd' (output path distribution), 'onewaycondition' (apply waypoint condition to each half of tract separately), 'waypoints=<white matter mask>' (paths must pass through white matter), 'cthr=0.2′ (curvature threshold), 'nsteps=2000′ (number of steps per sample), 'steplength=0.5′ (length of each step), 'nsamples=5000′ (total number of samples), 'fibthresh=0.01′ (threshold volume fraction to consider other fiber orientations), 'distthresh=0.0′ (discard samples shorter than 0.0 mm), and 'sampvox=0.0′ (sample random points within a sphere with this radius in mm from the center of the seed voxel). These parameters ensured that 5000 sample tracts were generated from the center of each voxel of each ROI and only tracts that (i) reached a target ROI and (ii) passed through white matter were retained. Note that no termination mask was used, because use of a termination mask when using the "network" flag (which is necessary to compute connectivity matrices between all pairs of ROIs) results in an empty matrix. This would occur because a termination mask would force streamlines to terminate when they reach any of the seed masks, including the mask it originates from. Thus, the use of termination masks would result in the streamlines never leaving the seed voxel. This resulted in a 186 × 186 connectivity matrix (per hemisphere) for each participant, where each entry represented the streamline count between each pair of nodes. Importantly, streamline count covaries with both the number of axons connecting two regions and the microstructural integrity of those axons (Donahue et al., 2016; Jbabdi and Johansen-Berg, 2011). The diagonal elements of the matrices represent self-connections and were excluded from analyses. To account for variability related to differences in ROI size within and across individuals and differences in the ability of tractography to reconstruct different white matter pathways (Brown et al., 2017), the retained (i.e., not rejected by inclusion and exclusion criteria) streamline counts originating from each seed ROI were divided by the total number of tracts that were retained for that ROI (Warrington et al., 2020). Thus, each of the resulting values reflects the proportion of streamlines originating from the seed ROI that connects to each of the other ROIs. Due to the tracking algorithm, the upper and lower diagonals of the initial connectivity matrix are not symmetric. However, because dMRI cannot detect directionality, the number of tracts from seed region A to target region B should be equivalent to that from seed region B to target region A. To correct for this, the matrix was symmetrized by averaging the number of tracts of the two matrix elements representing the same connection.

Given that probabilistic tractography tends to overestimate connectivity (Sotiropoulos and Zalesky, 2019), matrices were thresholded at 0.00005 to remove spurious connections. The use of such a

conservative threshold ensures that genuine connections are not removed, while still allowing for the removal of many spurious values.

2.7. Data analysis

2.7.1. Identification of direct amygdala connections

Direct network connections of amygdala were determined by creating a cross-sample network within hemisphere in order to classify nodes identified in later analyses as directly vs. indirectly connected. As mentioned above, probabilistic tractography tends to overestimate connectivity, and thus several steps were taken to maximize overall accuracy. First, connections that were not present across 80% of participants were excluded - the 80% threshold was chosen in light of research indicating that this threshold minimizes overall error (i.e., false positive + false negatives; Buchanan et al., 2020; de Reus and van den Heuvel, 2013). Second, the edge weight for each of the retained connections was averaged across participants to create a mean connectivity matrix, and the resultant matrix was used to create a minimum spanning tree (MST). An MST is a subgraph that connects all nodes using the minimum number of edges, thus ensuring overall connectivity. Finally, to remove the remaining spurious, noisy, and weak connections, the network was thresholded to achieve an overall density of 25%. We examined a range of density thresholds, and 25% was chosen as being the most consistent with known neuroanatomy. However, given that the choice of a 25% threshold was somewhat arbitrary, we have indicated when the results differed at a more conservative (i.e., 20%) or liberal (i.e., 30%) threshold. Density thresholding was carried out by adding edges to the MST backbone in order of decreasing edge weight. That is, edges with the largest weights were added to the backbone first until a network density of 25% was reached. In contrast to simply deleting edges with the lowest weights until a network density of 25% is reached, this method ensures that the network remains connected (Alexander-Bloch et al., 2010).

2.7.2. Identification of nodes vital to amygdala function

To identify nodes that are crucial for amygdala to function efficiently, we employed a novel 'virtual lesion' method using the matrices obtained after the initial 0.00005 threshold (note that these matrices did not undergo the MST procedure, nor the 25% density thresholding). As discussed above (and see Fig. 1), this method entails (i) calculating measures of amygdalar centrality in the full network, (ii) iteratively excluding each satellite node from the network and recalculating amygdalar centrality after each exclusion, and (iii) comparing amygdalar centrality with and without each satellite node. This process was repeated 185 times (once per satellite node) per participant, per hemisphere, per metric, per focal node. This was computed for all nodes in the network, rather than only the two nodes of interest – left and right amygdala – as these values were needed for normalization (discussed below). Rather than actually removing a satellite node from the network (which would leave the full and reduced networks at different sizes, which may bias property computation), we left the satellite node in the network and set all links that were greater than 0 for that node to the smallest floating-point number available in MATLAB (2.2251×10^{-308}). Setting links to this small number, rather than 0, was done, because setting them to 0 would leave the satellite node (and thus the network) disconnected, leaving the matrix without a unique inverse, which is needed for the computation of several properties. To ensure that the use of 2.2251×10^{-308} did not introduce inaccuracies during matrix inversions, we recomputed using 10×10^{-200} and 10×10^{-100}. Difference values were identical out to rounding error, indicating that our specific choice of number did not cause biased results. In summary, this method identifies nodes that, when 'lesioned', decrease the centrality of the amygdala, thereby identifying the network of satellite nodes crucial to supporting each amygdalar network property.

Two *a priori* normalizations were then applied within each participant to the centrality change values in order to facilitate valid interpretations of findings and comparisons across metrics. First, centrality change values were each divided by the (absolute value of the) mean (across focal nodes) for the removed (satellite) node and then values were mean centered (across focal nodes). Thus, this normalization was applied *within* each satellite node and *across* focal nodes. For example, the value for left amygdala (as the focal node) associated with removing left hippocampus (as the satellite node) was divided by the mean (across all focal nodes) of the change values associated with removing left hippocampus. This down-weighted the impact of satellite nodes that had a sizable impact on a large number of focal nodes across the brain, but whom are not specifically impactful on amygdala (i.e., their removal does not have a greater impact on amygdala than on most other nodes). Given that the goal of this study was to identify the network of regions crucial for *amygdalar* function, this normalization was carried out to ensure that the satellite nodes identified were specifically important for amygdala.

The second normalization consisted of dividing by the (absolute value of the) mean (across satellite nodes) value for the focal node and then mean (across satellite nodes) centering. Thus, the second normalization was applied *within* each focal node and *across* satellite nodes. For example, the value for left amygdala (as the focal node) associated with removing left hippocampus (as the satellite node) was divided by the mean (across all satellite nodes) of the change values. This was done to reduce the dependence of the metric change on changes in basic network properties. Specifically, before this normalization, change values were correlated with the simple reduction in mean link strength for the removed satellite node. In other words, satellite nodes that had overall stronger connections also tended to have larger reductions in the metric under investigation. This made it impossible to know whether findings were driven by aspects of the specific metrics or were simply due to the satellite node being strongly connected. Importantly, normalization reduced these correlations to near 0, thus allowing us to make interpretations about the actual properties investigated. Although perhaps not obvious, reducing these correlations to near 0 is particularly important for valid comparisons among properties. Specifically, each of the three graph properties may be more or less related to node strength. Thus, without normalization, comparisons between properties may be driven by the differential relationships with node strength itself. As an extreme example, pretend that subgraph values are highly related to node strength, but betweenness has no relationship with node strength. In this case, subgraph may be at an advantage (or disadvantage) in comparisons between the two, given that these values are driven by both the variance related to node strength and variance that is specific to subgraph, whereas betweenness values are driven only by the property itself. In addition, the final mean centering adjusted the values such that deviations from zero reflected shifts from the average impact of removing that node on all focal nodes. Interpretively, negative change values indicate that the removed node decreases the centrality of the focal node more than the average network node. Both normalizations also reduced the impact of participants with extreme values by standardizing their overall change values.

Perhaps most importantly, both normalizations also placed the three properties on the same scale to facilitate comparisons among them. As mentioned above, both normalizations were applied *within* each participant, and there are two reasons why this strategy is more advantageous than typical methods for placing variables on the same scale (e.g., *z*-scoring). First, it uses a greater amount of information (i.e., the change values for other focal/satellite node pairs, which are all on the same scale as the variable being normalized), leading to a more sensitive standardization. Second, the standardization is performed within each participant (rather than across participants, as done in *z*-scoring), and thus the impact of normalization is not dependent on the impact of the particular sample. For example, the value for a specific participant after *z*-scoring will change depending on the other participants used in the *z*-scoring, which is not true for our normalization procedure. Thus,

if *z*-scoring was used instead, comparisons between properties would be more dependent on the particular sample examined.

Normalized change values were then recursively winsorized (across participants) for each metric to ±3 standard deviations in order to rein-in outliers. This treatment of outliers was carried out *a priori*. Additionally, all regions identified in the main analyses remained the same regardless of whether or not data was first winsorized.

To conduct a stringent test of regions critical to supporting amygdalar functionalities, participants were randomly grouped into ten sets with 105 or 106 participants in each set. For each set, change values were entered as dependent variables in robust two-sided *t*-tests in the Graph Theory GLM (GTG) toolbox (Spielberg et al., 2015) to determine whether the differences between the properties calculated with the full and reduced matrices were significant. In addition, for each set, change values were entered pairwise (e.g., *node communicability* and *subgraph centrality*) as dependent variables in *F*-tests, as described above, to determine whether changes in two metrics were significantly different from each other. Significance was determined via permutation tests (7500 repetitions), and false discovery rate (FDR) was used to correct for multiple comparisons across nodes (Benjamini and Hochberg, 1995). Adjusted *p*-values were considered significant if less than the *q*-value of 0.05. Critical *p*-values for each statistical test are reported in Supplementary Table 5.

Scripts for computation of graph properties and 'virtual lesioning' are available on the last author's website (https://sites.udel.edu/jmsp/tools_data/) and by request, and will be part of a future release of the GTG toolbox (www.nitrc.org/projects/metalab_gtg). Data included in this manuscript were obtained from the Human Connectome Project (Young Adult), publicly available at https://www.humanconnectome.org/study/hcp-young-adult. Connectivity matrices derived from the HCP data are available on the last author's website (https://sites.udel.edu/jmsp/tools_data/).

3. Results

3.1. Identification of direct amygdalar connections

In order to classify satellite nodes as directly (vs. indirectly) connected to the amygdala, we created within-hemisphere networks. Only those connections that were present in at least 80% of subjects were retained. Thus, 'direct connections' are those that retained connectivity with the amygdala after this 80% thresholding, and nodes not identified in this analysis were assumed to be indirectly connected to the amygdala. The left amygdala was directly connected to 42 nodes (black lines in Supplementary Fig. 1), including Brodmann areas 13l, 45, 47l, 47 s, 7PL, and a47r; anterior agranular insular, entorhinal, perirhinal-ectorhinal, orbitofrontal (OFC), parahippocampal, piriform, retrosplenial, temporopolar, and visual cortices 1, 2, 3, 3A, 4, 6, 6A, and 7; nucleus accumbens, caudate, pallidum, putamen, thalamus, hippocampus, dorsal visual transition area, anterior inferior frontal junction, lateral occipital area 3, angular gyrus, supramarginal, posterior OFC, posterior insula, parieto-occipital sulcus, presubiculum, and prostriate area. The right amygdala as directly connected to 54 nodes (black lines in Supplementary Fig. 2), including Brodmann areas 10pp, 10v, 25, 33pr, 47l, 47 s, 7Am, 7PL, 7Pm, a10p, a24, a47r, and s32; entorhinal, perirhinal-ectorhinal, parahippocampal, piriform, retrospenial, temporopolar, and visual cortices 1, 2, 3, 3A, 4, 4t, 6, 6A, 7; nucleus accumbens, caudate, pallidum, putamen, thalamus, hippocampus, dorsal visual transition area, anterior inferior frontal junction, lateral occipital area 2, OFC, premotor eye field, angular gyrus, supramarginal, posterior inferotemporal complex, posterior OFC, parieto-occipital sulcus, presubiculum, prostriate area, temporal fusiform, ventral intraparietal complex, and ventromedial visual area. Satellite nodes that were found to be vital to amygdalar network properties are classified as directly (vs. indirectly) connected to the amygdala (see Tables 1–3).

3.2. Identification of nodes vital to amygdalar network properties

Using our novel 'virtual lesioning' procedure described above, we measured the extent to which a node supports amygdalar network properties. In particular, we examined amygdalar centrality with (full network) and without (reduced network) that node. The relative change in amygdalar centrality (full vs. reduced) reflects the importance of the removed satellite node for that amygdalar network property. We found that amygdalar *CF betweenness* was significantly reduced (across all 10 sets of participants) after removal of 59 (left) and 64 (right) of the 186 satellite nodes examined. Similarly, removal of 9 (left) and 11 (right) regions were associated with significant reductions in amygdalar *node communicability* across all sets, and removal of 104 (left) and 105 (right) regions were associated with significant reductions in amygdalar *subgraph centrality* across all sets (all p's < 0.05 after multiple comparisons correction; see Supplementary Tables 1 and 2).

3.3. Between-metric comparison of identified nodes

To determine whether a satellite node was more important for one centrality metric than others, we compared the impact of each node identified by a given metric to the impact of that node for the other two metrics via *F*-tests. For example, for those nodes identified in earlier analyses as supporting amygdalar *CF betweenness* (i.e., a significant reduction in amygdala *betweenness* was observed after removing the node), we tested whether the reduction in amygdalar *CF betweenness* (after removing the node) was greater than the reductions in *node communicability* and *subgraph centrality* (after removing that same node). In other words, these tests allowed us to identify the set of regions that were specifically important for supporting each type of amygdala influence examined. These tests were again conducted within each of the 10 sets of participants, and only regions that were significant across all sets were retained.

The sets of regions evidencing significant between-metric tests are listed in Tables 1–3 and Figs. 5 and 6. Across all sets, 13 (left) and 12 (right) regions showed greater reductions for *CF betweenness* (Table 1; all p's < 0.05 after correction for multiple comparisons) than the other two metrics, indicating that these regions are particularly crucial for supporting this aspect of amygdalar processing. These regions included visual cortex (V2, V3, V6), insula (parainsular cortex, posterior insula, anterior agranular insula complex), putamen, medial temporal lobe (parahippocampus, retrosplenial cortex), prostriate area, temporal fusiform, parietal-occipital sulcus, BA 7Pm, anterior superior temporal gyrus, and inferior frontal cortex (lateral BA 47, posterior BA 47r, anterior inferior frontal sulcus). Similarly, 7 (left) and 7 (right) regions showed greater reductions for *node communicability* (Table 2) than the other two metrics. These regions included thalamus, striatum (pallidum, nucleus accumbens), piriform cortex, thalamus, and medial temporal cortex (perirhinal-ectorhinal cortex, entorhinal cortex, temporopolar cortex).

Lastly, 82 (left) and 83 (right) regions showed greater reductions for *subgraph centrality* (Supplementary Tables 3 and 4) than the other two metrics. Given that discussion of the large number of regions found for *subgraph centrality* would be unwieldy, we focus on only the nodes that had one of the top 25% (satellite nodes analyzed) highest F-values for *subgraph centrality* in the analyses comparing change in *subgraph centrality* for a given satellite node to 0 (e.g., Supplementary Tables 1 and 2). This approach allowed us to identify nodes that showed consistently strong impacts on amygdalar *subgraph centrality* across sets, which resulted in 12 (left) and 11 (right) regions (Table 1). Note that the choice of the top 25% is arbitrary – this value was chosen as it resulted in a number of nodes that was similar to the other two metrics and thus manageable to discuss. These regions included somatosensory cortex, auditory areas (A4, A5), visual areas (V4), superior temporal sulcus, intraparietal area, posterior insula, frontal operculum, inferior supramarginal gyrus, temporo-occipital and posterior middle temporal gyrus,

Table 1
Set of satellite nodes showing differentially stronger impact for amygdala current-flow betweenness centrality.

Satellite (Removed) Node Descriptive Name	HCP Name	Direct?	ΔMetric v 0 Avg. t	BC v NC Avg. F	BC v SC Avg. F
Left Posterior insula	PoI2	Y	75.2***	445.2***	42.3***
Left Putamen	–	Y	67.6***	6.0*	1001.5***
Left Anterior agranular insular cortex	AAIC	Y	34.1***	63.8***	10.7***
Left Posterior-medial BA7	7Pm	N[b]	33.0***	393.7***	56.3***
Left Parainsular cortex	PI	N	32.1***	18.7***	29.6***
Left Parieto-occipital sulcus	POS2	Y	24.4***	8.1***	10.6***
Left Lateral BA47	47l	Y[a]	20.5***	7.9***	26.0***
Left Visual area 3	V3	Y	10.4***	23.1***	47.4***
Left Para-hippocamal area	PHA1	Y	8.5***	281***	27.2***
Left Prostriate area	ProS	Y	7.8***	13.7***	34.4***
Left Visual area 2	V2	Y	7.5***	261.1***	97.4***
Left Para-hippocampal area	PHA3	Y[a]	4.8***	359.6***	15.2***
Left BAp47r	p47r	N	3.5*	46.4***	32.5***
Right Parainsular cortex	PI	N	26.0***	15.9***	7.8*
Right Posterior-medial BA7	7Pm	Y[a]	25.3***	34.5***	24.5***
Right Lateral BA47	47l	Y[a]	17.3***	14.7***	11.1***
Right Posterior BA47r	p47r	N[a]	16.9***	114.4***	163.5***
Right Anterior superior temporal gyrus	STGa	N[b]	13.6***	24.9***	12.1***
Right Visual area 3	V3	Y	12.2***	12.3***	22.3***
Right Parahippocampal area	PHA1	Y	9.5***	281.5***	94.6***
Right Anterior inferior frontal sulcus	IFSa	N[b]	8.1***	69.5***	17.5***
Right Parahippocampal area	PHA3	Y	8.0***	516.1***	17.1***
Right Retrosplenial cortex	RSC	Y	6.4**	21.4***	17.7***
Right Visual area 2	V2	Y	5.7**	261.7***	103.0***
Right Temporal fusiform	TF	Y[a]	4.7*	18.4***	10.8***
Right Visual area 6	V6	Y[a]	3.3*	66.1***	82.6***

Note. ΔMetric v 0 = test that change in metric (reduced vs. full) is different from 0; BC v NC = test that change in CF betweenness is different from change in node communicability; BC v SC = test that change in CF betweenness is different from change in subgraph centrality; $^{*}p < .05$, $^{**}p < .01$, $^{***}p < .001$; all reported *ps* are the maximum across all 10 sets after false discovery rate correction; Connect Directly = region identified as directly connected to amygdala with MST density = 25%; [a] with MST density = 20% region is indirect; [b] with MST density = 30% region is direct; HCP Name = label from Human Connectome Project atlas; Avg. *t* = average t statistic across all 10 sets; Avg. *F* = average F statistic across all 10 sets; BA = Brodmann's area.

Table 2
Set of satellite nodes showing differentially stronger impact for amygdala node communicability.

Satellite (Removed) Node Descriptive Name	HCP Name	Direct?	ΔMetric v 0 Avg. *t*	BC v NC Avg. *F*	BC v SC Avg. *F*
Left Thalamus	–	Y	15.8***	58.4***	70.8***
Left Perirhinal ectorhinal cortex	PeEc	Y	10.5***	23.0***	35.3***
Left Dorsal temporal pole	TGd	Y	9.0***	14.6***	16.9***
Left Piriform cortex	Pir	Y	6.9***	14.3***	17.8***
Left Nucleus accumbens	–	Y	6.4***	23.6**	27.9***
Left Entorhinal cortex	EC	Y	5.9***	8.7***	11.4***
Left Ventral temporal pole	TGv	Y	5.1***	9.1*	16.4***
Right Thalamus	–	Y	18.5***	140.8***	176.7***
Right Dorsal temporal pole	TGd	Y	12.3***	29.0***	31.2***
Right Perirhinal-ectorhinal cortex	PeEc	Y	11.7***	27.2***	26.0***
Right Entorhinal cortex	EC	Y	8.2***	13.8**	16.2**
Right Pallidum	–	Y	8.1***	15.6***	18.1***
Right Ventral temporal pole	TGv	Y	6.8***	16.4***	17.3***
Right Nucleus accumbens	–	Y	5.3***	10.2***	9.3***

Note. ΔMetric v 0 = test that change in metric (reduced vs. full) is different from 0; BC v NC = test that change in CF betweenness is different from change in node communicability; NC v SC = test that change in node communicability is different from change in subgraph centrality; $^{*}p < .05$, $^{**}p < .01$, $^{***}p < .001$; all reported *ps* are the maximum across all 10 sets after false discovery rate correction; Connect Directly = region identified as directly connected to amygdala with MST density = 25%; HCP Name = label from Human Connectome Project atlas; Avg. *t* = average t statistic across all 10 sets; Avg. *F* = average F statistic across all 10 sets; BA = Brodmann's area.

Table 3
Set of satellite nodes showing differentially stronger impact for amygdala subgraph centrality.

Satellite (Removed) Node Descriptive Name	HCP Name	Direct?	ΔMetric v 0 Avg. *t*	BC v NC Avg. *F*	BC v SC Avg. *F*
Left Auditory area 4	A4	N	68.2***	397.4***	40.3***
Left Ventral BA8A	8Av	N	49.1***	126.1***	97.3***
Left Auditory area 5	A5	N	38.7***	121.5***	31.1***
Left Temporo-occipital medial temporal gyrus	PHT	N	38.2***	192.4***	41.9***
Left Inferior supramarginal gyrus	PFm	N	36.1***	75.7***	19.2***
Left Middle BA9	9m	N	30.7***	80.4***	13.8***
Left Posterior middle temporal gyrus	TE1p	N	26.8***	38.4***	42.2***
Left BA1	1	N	21.1***	25.3**	28.4***
Left BA44	44	N	15.9***	20.6***	29.3***
Left BA10d	10d	N[b]	15.6***	43.3***	18.4***
Left Visual area 4	V4	Y	15.1***	57.0***	47.8***
Left Frontal opercular area	FOP2	N	11.3***	55.7***	23.8***
Right Auditory area 4	A4	N	56.9***	364.7***	50.6***
Right Posterior insula	PoI2	N	49.5***	47.4***	519.1***
Right Auditory area 5	A5	N	39.7***	155.3***	40.5***
Right BA1	1	N	37.7***	175.6***	17.1***
Right BA44	44	N	26.2***	37.8**	21.3***
Right Medial BA9	9m	N	23.8***	80.3***	14.4***
Right BA4	4	N	19.5***	56.3***	12.8***
Right Posterior BA24	p24	N[b]	14.9***	96.2***	30.7***
Right Intraparietal area	IP1	N[b]	14.2***	41.8***	14.6***
Right Dorsal posterior superior temporal sulcus	STSdp	N	12.3***	720.2***	19.4***
Right Posterior inferior frontal junction	IFJp	N	10.1***	684.4***	19.3***

Note. ΔMetric v 0 = test that change in metric (reduced vs. full) is different from 0; BC v NC = test that change in CF betweenness is different from change in node communicability; NC v SC = test that change in node communicability is different from change in subgraph centrality; $^{*}p < .05$, $^{**}p < .01$, $^{***}p < .001$; all reported *ps* are the maximum across all 10 sets after false discovery rate correction; Connect Directly = region identified as directly connected to amygdala with MST density = 25%; [a] with MST density = 20% region is indirect; [b] with MST density = 30% region is direct; HCP Name = label from Human Connectome Project atlas; Avg. *t* = average t statistic across all 10 sets; Avg. *F* = average F statistic across all 10 sets; BA = Brodmann's area.

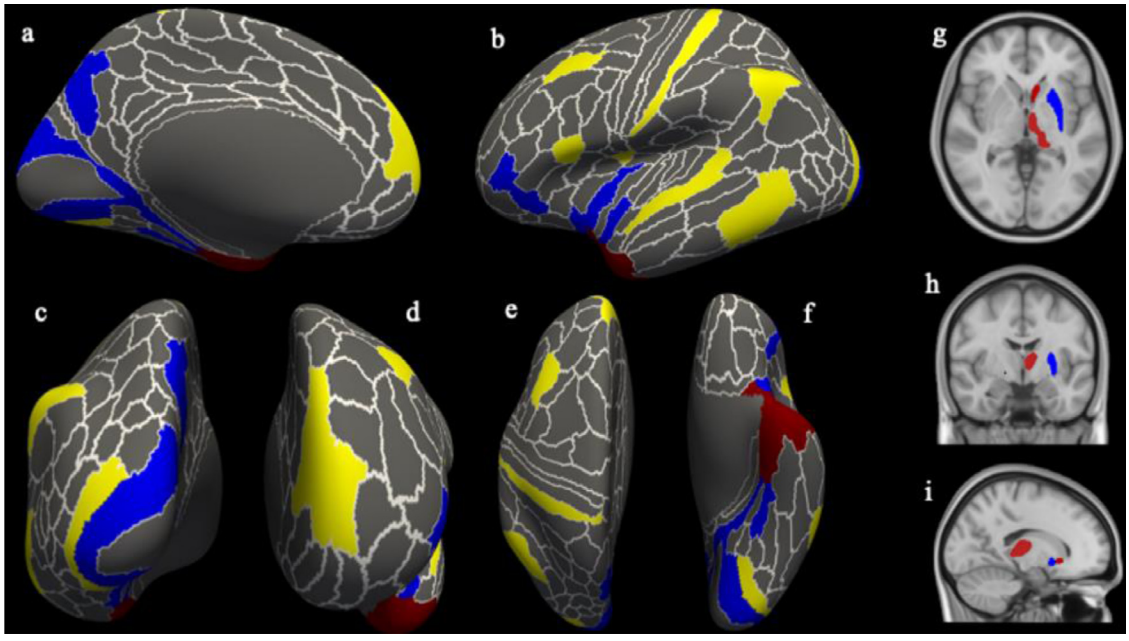

Fig. 5. Between-metric comparison of identified nodes in left hemisphere.
Regions supporting amygdalar current-flow betweenness centrality shown in blue, node communicability shown in red, subgraph centrality shown in yellow. (A–F) cortical regions, (G–I) subcortical regions. (A) medial view, (B) lateral view, (C) posterior view, (D) anterior view, (E) superior view, (F) inferior view, (G) axial view, (H) coronal view, (I) sagittal view.

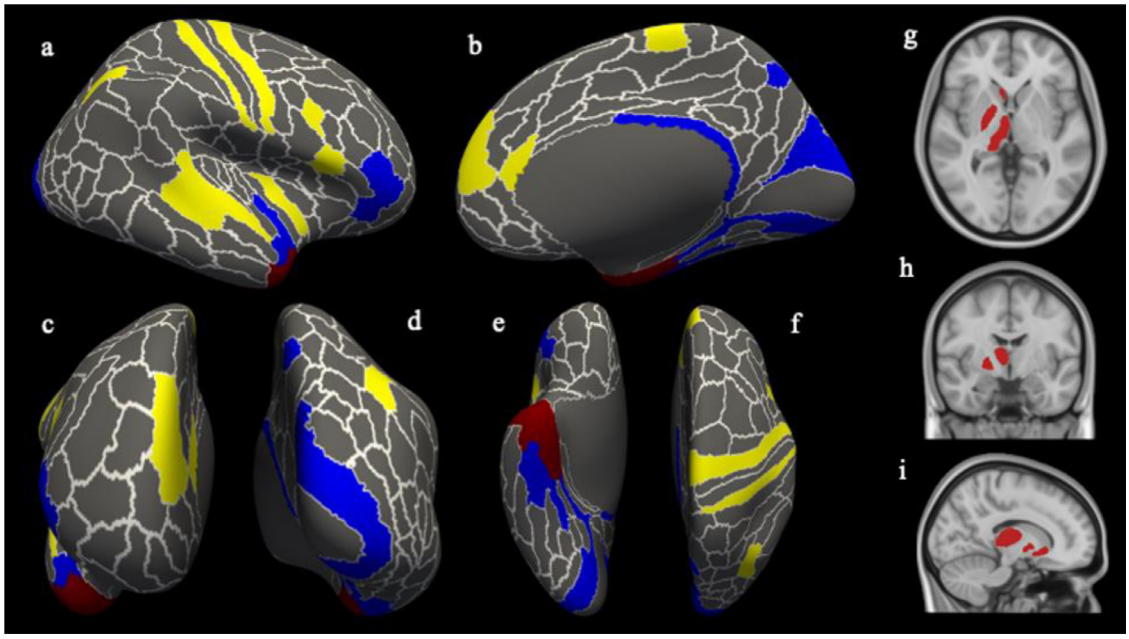

Fig. 6. Between-metric comparison of identified nodes in right hemisphere.
Regions supporting amygdalar current-flow betweenness centrality shown in blue, node communicability shown in red, subgraph centrality shown in yellow. (A–F) cortical regions, (G–I) subcortical regions. (A) lateral view, (B) medial view, (C) anterior view, (D) posterior view, (E) inferior view, (F) superior view, (G) axial view, (H) coronal view, (I) sagittal view.

and posterior prefrontal cortex (BA 9 m, BA 8Av, BA 44, BA 10d), and pregenual ACC. All other results available in Supplementary Tables 1–4.

4. Discussion

Networks are the chief organizational principle of the brain. Consequently, the capability of a specific region cannot be understood without first identifying the set of structures that allow these capabilities to emerge. The goal of the present work was to identify brain structures that support the amygdala's ability to effectively influence the larger brain network via three different modes of communication. Present findings were derived from the application of a novel technique wherein we compared graph theory metrics assaying different types of amygdalar network communication (i.e., centrality) that were derived from the full network to those same metrics after removing a 'satellite' (i.e., non-amygdala) network node. This allowed us to identify nodes whose removal caused large drops in amygdalar centrality, and thus, appear to be critical to the amygdala's ability to influence (or be influenced by) the network. This approach is in contrast to conventional methods, which focus on either (i) connectivity between regions or (ii) the importance of a specific region. Even past 'virtual lesion' methods provide insight only into how a single region impacts the global network. The technique introduced herein provides information not available with these methods – namely, insight into the specific (sets of) regions that *allow the amygdala to function effectively*. In other words, this method identifies the 'support network(s)', as it were, that provide the amygdala with the framework needed to carry out its different functions. Moreover, this novel method can be used to identify separate 'support networks' associated with different aspects of amygdalar communication, including the quality (i.e., signal-to-noise) and level of influence of these signals. Overall, present findings show that there is no single 'amygdalar network'. Rather, our findings indicate, for the first time, that there are several 'amygdala networks', each of which is critical for a unique aspect of network communication by which the amygdala interacts with the greater network. For example, regions supporting amygdalar *betweenness* and *communicability* were associated with the anterior and posterior systems, respectively, identified in previous work as supporting distinct aspects of memory-guided behavior (Ranganath and Ritchey, 2012).

4.1. Novel contribution of the new method

Although some of the regions identified herein have long been known to interact with the amygdala in significant ways, the present work provides independent evidence for the importance of these regions, because the techniques employed herein determine importance solely based on the positions of these regions (relative to the amygdala) within the larger brain network. Moreover, the present findings provide unique insights into *why* these regions are important to amygdalar functioning. Our method helps to answer this question by identifying the *modes of network communication* that are disturbed when a given region is virtually lesioned. Thus, the fact that the proposed method identified many regions known from past work to interact with the amygdala in significant ways is supportive of the validity of our method. Furthermore, the present work integrates the roles of both direct and indirect (i.e., physically connected to amygdala via another node(s)) connections, affording an exponentially more complex understanding of amygdalar networks relative to direct connectivity only or bivariate approaches. Hence, present findings enrich our understanding of the amygdala's capability to interact with other brain regions, through which complex psychological processes emerge.

To illustrate the new insights that our method provides, we highlight a few results for each graph property. As the majority of regions identified herein have been linked to multiple types of psychological processes, we cannot know which of these processes is important for supporting amygdalar network processes. However, to provide context for the new insights of present findings, we speculate below regarding the potential ways in which these regions support different aspects of amygdalar processing, and further research is needed to support/refute these ideas. Note that we limit discussion to those 'satellite' nodes that emerged as significantly more important for a given property compared to the other two. The HCP atlas name for each node is given in parentheses/brackets when regions are first mentioned.

4.2. Current-flow (CF) betweenness centrality

CF betweenness centrality reflects the extent to which a node influences information flow between all pairs of nodes in the network. Thus, reductions in amygdalar *CF betweenness centrality* after a satellite node is removed indicate that the removed node functions as a bottleneck for information flowing to or away from the amygdala, reducing the amygdala's ability to serve as a global network hub of information flow in the brain. For a region to function as a bottleneck, alternate paths for information flow to the amygdala must be limited.

Amygdalar *CF betweenness* was associated with parahippocampal (PHA1, PHA3, TF) and retrosplenial (RSC, POS2) cortices, which form the Posterior Medial Memory System, one of two separable systems supporting memory-guided behavior. The Posterior Medial Memory System mediates information flow to the entorhinal cortex and hippocampus to support functions such as episodic memory and spatial navigation, whereas the Anterior Temporal Memory System is associated with affective aspects of memory (Ranganath and Ritchey, 2012). Our finding that the parahippocampal and retrospenial cortices support amygdalar *CF betweenness* suggests that these regions promote amygdalar influence over global network communication. For example, amygdala may exert influence over the encoding and retrieval of episodic memories via its influence over network communication flowing through parahippocampal and retrospenial cortices, despite amygdala lacking direct associations with the Posterior Medial Memory System (Ranganath and Ritchey, 2012). Interestingly, as discussed below, *node communicability* was associated with regions in the Anterior Medial Memory System, suggesting that these systems support separable aspects of amygdalar interactions with the network.

Additionally, several regions of the orbital inferior frontal cortex (IFC) emerged as crucial for supporting amygdalar *CF betweenness*. As mentioned above, reductions in amygdalar *CF betweenness* after a node in IFC is removed indicate that these IFC regions support amygdalar influence over network communication by facilitating information flow between the amygdala and the larger network. This is consistent with the known connectivity profile of the orbital inferior frontal gyrus (*pars orbitalis*: lateral BA 47 [47l], posterior BA 47r [p47r]; anterior inferior frontal sulcus [IFSa]), which is directly connected to the amygdala via uncinate fasciculus (Catani et al., 2002) and is thought to be a 'neural hub' where semantic and emotion expression networks intersect (Belyk et al., 2017). Present findings extend previous work by suggesting that the orbital IFC facilitates amygdalar influence over communication with the rest of the network, particularly other regions of prefrontal cortex (PFC). Specifically, the orbital IFC may support the influence of amygdalar signals within the global network by mediating the flow of amygdalar information regarding the perception of semantic and emotional content to other PFC regions.

4.3. Node communicability

Changes in amygdalar *node communicability* after a satellite node is removed indicate that the removed node impacts the amygdala's ability to send and receive information clearly (i.e., without interference) to/from other parts of the network. In particular, *node communicability* indexes the number of different (parallel) paths that information can travel between the amygdala and other nodes. Having multiple paths through which to transmit information improves signal clarity, because information traveling along multiple paths will, on average, reduce the impact of noise added along each individual pathway (Benzi and Klymko, 2013; Estrada and Hatano, 2008). Thus, if a satellite node is identified as critical for supporting amygdalar *communicability*, it likely serves as a gateway through which amygdala accesses multiple paths. A limitation of this interpretation is that the existence of more paths may not lead to clearer information transfer under all conditions (e.g., when there are similar sources of noise across multiple paths).

The thalamus was found to facilitate amygdalar *node communicability*, suggesting that the thalamus serves as a gateway through which many types of information must pass to reach the amygdala and/or as a key output pathway for the amygdala to influence the network. Although previous studies have shown that the thalamus projects to the amygdala (Vertes et al., 2015), present findings provide novel insights into the manner in which the thalamus is important to the amygdala. Specifically, our findings suggest that information sent to the thalamus by the amygdala is retransmitted widely, increasing the clarity of information sent by the amygdala through other routes (i.e., same information arriving via multiple paths). This is consistent with the wealth of prior evidence indicating that the thalamus is connected to a wide array of inputs (Kumar et al., 2015), along with work suggesting that the thalamus and amygdala interact during emotion processing (LeDoux, 2000; Tamietto and De Gelder, 2010). Present findings extend this understanding by indicating that the thalamus interacts with amygdala by promoting the clear communication of amygdalar signals via parallel communication pathways. Additionally, the thalamus is critical to the reorganization of sensory information from the environment before such information reaches the cortex (Tyll et al., 2011). Given present findings, input from the amygdala encoding the salience of environmental information may, via the thalamus, modulate sensory information that is sent to the cortex, and thus, boost the transmission of amygdalar signals.

Amygdalar *communicability* was also found to be supported by the perirhinal-ectorhinal (PeEc), entorhinal (EC), and temporopolar (TGd; TGv) cortices. These regions form the Anterior Temporal Memory System, which is associated with guiding behavior based on affective aspects of memory (Ranganath and Ritchey, 2012). This system is thought to directly interact with amygdala via strong direct anatomical connections with PeEc and EC (McDonald, 1998; Stefanacci et al., 1996) which support the assignment of salience to situations and objects (Ranganath and Ritchey, 2012). Present findings using our 'virtual lesion' method provide deeper insights into established associations between the amygdala and the Anterior Temporal Memory System. In particular, our findings suggest that the PeEc, EC, TGd, and TGv support amygdalar influence on memory systems by *promoting the clarity* of amygdalar signals within that network. Present findings also provide additional insights into how the Anterior Temporal and Posterior Medial Memory Systems operate as separate entities, with regard to amygdala, in addition to how amygdala and these systems interact with each other as a circuit. In particular, present findings extend previous work by indicating that the Anterior Temporal Memory System promotes amygdalar communication via high-quality information flow (*communicability*) and the Posterior Medial Memory System promotes the influence of amygdalar signals over global network processing (*CF betweenness*).

4.4. Subgraph centrality

Changes in amygdalar *subgraph centrality* after a satellite node is removed indicate that the removed node impacts the extent to which amygdala influences communication in local networks via recurrent processing that reincorporates amygdala-related information. In particular, *subgraph centrality* indexes the number of different self-loops (paths that start and end at amygdala). The more self-loops in the local network, the more paths there are by which amygdala can influence that network. Thus, nodes whose removal results in a reduction in *subgraph centrality* are likely to be important hubs for creating amygdalar self-loops and serve as a gateway through which the amygdala influences local networks.

Several regions of PFC, including dorsomedial (9 m) and dorsolateral (8AV) PFC, were identified as critical to supporting amygdalar *subgraph centrality*, suggesting that they are important hubs for creating amygdalar self-loops. Although these regions are known to interact with the amygdala to support emotion conceptualization and regulation (Lindquist et al., 2012; Morawetz et al., 2017), previous research has not

identified the manner in which this interaction occurs within the network context. Thus, present findings extend previous work by indicating that these PFC regions promote the influence of amygdalar signals within local networks. For example, in the context of past work indicating that 9 m interacts with both amygdala and hippocampus during the encoding of salient experiences (Lindquist et al., 2012), present findings suggest that 9 m serves to funnel amygdalar signals back into this local network, potentially facilitating amygdalar modulation of memory encoding. Similarly, given that 8Av interacts with amygdala during emotion regulation (Morawetz et al., 2017), this region may reflect amygdalar signals back into local networks, based on contextual needs. It is important to recall that we are examining white matter networks, which provide insight into the possible ways in which networks *may* communicate, rather than how they do so in a particular context (which is likely better reflected in functional networks). Thus, our findings do not indicate that 8Av will *always* reflect back amygdalar signals, but rather will likely modulate the return (and thus amplification) of these signals based on regulatory needs.

4.5. Overall between-metric comparisons

In general, removal of satellite nodes had larger impacts (i.e., larger, more consistent effect sizes) on amygdalar *subgraph centrality* than on *CF betweenness* and *node communicability* (see Tables 1–3). One potential explanation is that, because local networks are smaller (i.e., fewer nodes), removal of nodes within such networks may have an outsized impact on local processing because it accounts for a larger share of network connections. Across the three amygdalar functions examined, groups of regions were identified that support memory functions (*betweenness*: parahippocampal and retrosplenial cortices; *communicability*: perirhinal, entorhinal and temporopolar cortices), a range of sensory-related regions that support relatively basic sensory processing (*betweenness*: visual cortex, *communicability*: piriform; *subgraph*: somatosensory cortex, auditory association areas) to higher-order sensory integration processes (*betweenness*: insula; *subgraph*: superior temporal sulcus, intraparietal area), and distinct frontal areas involved in various aspects of executive functions (*betweenness*: inferior frontal cortex; *subgraph*: dorsal PFC, inferior frontal gyrus, ACC). Thus, although the regions identified differed depending on the specific amygdalar function examined, together the three metrics identified regions that are consistent with known direct and indirect connections, providing independent evidence for the importance of these regions with known interactions with the amygdala and providing insights into which aspects of amygdalar communication they support.

4.6. Implications and potential extensions of the novel method

The current study demonstrated the utility of a novel method that (i) identifies nodes critical to the functionality of a brain region of interest (e.g., amygdala) and (ii), perhaps more importantly, provides insights into *the manner in which these nodes support the function of that region*. For example, it is well-established that dorsolateral PFC interacts with amygdala, likely in support of emotion regulation (Morawetz et al., 2017). Present findings, gained from our novel method, extend our understanding by indicating that the dorsolateral PFC contributes to the amygdala's ability to influence communication in local networks (*subgraph centrality*). Similarly, our finding that the orbital IFC is critical to the amygdala's ability to exert influence over global network communication (*CF betweenness*) adds to our existing understanding that the orbital IFC interacts with the amygdala to support emotion perception (Frank et al., 2019) by identifying the manner in which the orbital IFC contributes to amygdalar functionality.

The potential utility of this method is not restricted to diffusion-based structural networks but can be applied to any network in which basic assumptions are met (i.e., where there is a theoretically interpretable effect of removing a node from the network), including those derived from functional MRI. Furthermore, this method can be extended to the examination of individual differences. For example, past work using traditional methods support the existence of disturbed amygdalar function among those with pathological anxiety (Xu et al., 2019), but the source of this disturbance remains unclear. Our method could be employed to identify (i) which brain regions contribute to this disturbance and (ii) the specific methods of amygdalar network communication which are disturbed by these regions. Specifically, our method could be applied with the amygdala again as the focal node, but instead of examining mean centrality changes (due to node removal) across the sample, as done in the present study, one could test whether the extent of centrality change correlates with anxiety (or differs between anxious patients and healthy controls). Similar analyses could be undertaken to examine normative individual differences. For example, the proposed method could provide insight into inhibitory control capacity by identifying the nodes that support different types of dorsal anterior cingulate network communication. In summary, the proposed method has a wide array of potential uses that span multiple imaging modalities and areas of psychology, psychiatry, and neuroscience.

4.7. Strengths & limitations

The present study benefited from a number of strengths, including an extremely large sample size ($n = 1052$), multi-shell diffusion acquisition with a large number of directions ($n = 270$) which provided unparalleled accuracy in tractography, the use of an ROI atlas created using multiple imaging modalities, which is likely more accurate, and the use of cutting-edge, novel graph-theory methodology. Several limitations must also be considered. Although we used the best methods currently available, present findings are dependent on the connectivity algorithms used, and thus, it is possible that systematic biases remain. For example, the normalization that we applied to streamline counts (i.e., dividing retained streamline counts from each seed ROI by the total retained streamlines for that ROI) differentially impacts ROIs according to their size and thus may have introduced some bias. We used this procedure given that (i) it is the standard used in FSL and (ii) it removed variability within and among participants that is unrelated to current study goals and could confound differences of interest. However, future work could investigate the impact of such normalization on this method. Another potential limitation is the fact that we examined only three nodal graph metrics. Other metrics might provide important insights, and future research should expand beyond those used herein. A third potential limitation is the fact that we used streamline count as our index of connectivity strength, which are only indirect measures of such strength and not the only such measure available (e.g., fractional anisotropy). Thus, it is possible that a different index of connectivity strength would provide different findings. We chose to use streamlines, because past work has linked streamlines to connection strength values derived from tract tracing in monkeys (Donahue et al., 2016; van den Heuvel et al., 2015). In addition, networks based on streamlines appear to have higher reproducibility than those based on fractional anisotropy (Roine et al., 2019). A fourth potential limitation is the fact that, because directionality cannot be inferred from dMRI, the interpretations of the metrics must be assumed to be bidirectional. However, this assumption is not completely accurate as there are connections between brain regions that are not reciprocal. A fifth potential limitation is that, because tractography was performed between all ROI pairs, we were unable to use a termination mask. Thus, it is possible, although unlikely, that a given streamline could start at one region, travel *through* another region, and continue on to a third region. A sixth potential limitation is the resolution of the subcortical segmentation used (e.g., treating thalamus as a single structure). It is possible that the use of a different atlas with more subcortical divisions would produce different findings. However, we chose to use the standard FreeSurfer segmentation, because this is based on each participant's anatomy and thus likely to have a more accurate placement. Additionally, in a subsample ($n = 106$), we compared our method against a

different (registration-based) subcortical segmentation (along with the standard FreeSurfer cortical parcellation). We found that results for subgraph and communicability were extremely consistent, suggesting that present findings are not highly dependent on the choice of subcortical atlas. However, the results for betweenness using these two atlases were more variable (see Supplemental Material). Similarly, betweenness was the only metric that, in supplemental analysis, was found to vary by the threshold applied to connectivity matrices before calculation of graph metrics (see Supplemental Material). Together, these findings suggest that betweenness may be less robust to methodological differences, and thus, should be interpreted with some caution. A final potential limitation is the fact that the sample used was psychiatrically healthy, and thus present findings may not reflect organization within pathological populations (e.g., anxiety). However, the methods introduced herein can be used to examine the impact of individual differences on network organization.

5. Conclusion

The current study is the first delineation of the architecture supporting amygdalar network properties in the human brain. Using novel graph theory methods, we identified, for specific emergent communication properties of the amygdala, a network of nodes that are related to the amygdala's role in emotional and motivational processes such as evaluating the salience of stimuli, moderating attention to stimuli, and coordinating behavioral responses to stimuli. The specific regions identified herein are consistent with known direct and indirect amygdalar connections and differed depending on the specific amygdalar function examined (i.e., amygdalar influence over local networks [*subgraph centrality*], clarity of amygdalar communication with network nodes [*node communicability*], amygdalar influence over information flow between other nodes [*betweenness centrality*]), supporting the specificity of these findings. In particular, present findings expand our current understanding by identifying the manner in which regions are important to amygdala, in addition to showing that there is no single 'amygdalar network', but rather several networks, each of which supports a different way in which the amygdala exerts influence over the brain network.

The methodology developed for the present study leveraged the *unique position* each satellite node occupied in the network to determine their contribution to supporting amygdalar influence over the network. In turn, this provides a normative framework of amygdalar networks that open several lines of inquiry. For example, as discussed above, future research could examine the manner in which pathological amygdalar processes arise (e.g., by identifying deviations from this framework). In summary, the findings presented herein (i) advance our knowledge of how amygdalar function depends upon the concerted activity of a complex network of directly and indirectly connected nodes and (ii) support the validity of a novel method that allows for the investigation of how brain regions support a region of interest.

Declaration of Competing Interest

None.

Credit authorship contribution statement

Melanie A. Matyi: Conceptualization, Methodology, Formal analysis, Visualization, Writing – original draft. **Sebastian M. Cioaba:** Software. **Marie T. Banich:** Writing – review & editing. **Jeffrey M. Spielberg:** Conceptualization, Methodology, Software, Writing – review & editing, Resources, Supervision.

Acknowledgments

Research of Sebastian M. Cioaba is partially supported by the National Science Foundation [Grant Nos. DMS-1600768, CIF-181592] and the Japanese Society for the Promotion of Science [Fellowship]. Data were provided by the Human Connectome Project, WU-Minn Consortium (Principal Investigators: David Van Essen and Kamil Ugurbil; 1U54MH091657) funded by the 16 NIH Institutes and Centers that support the NIH Blueprint for Neuroscience Research; and by the McDonnell Center for Systems Neuroscience at Washington University.

Supplementary materials

Supplementary material associated with this article can be found, in the online version, at doi:10.1016/j.neuroimage.2021.118614.

References

Alexander-Bloch, A.F., Gogtay, N., Meunier, D., Birn, R., Clasen, L., Lalonde, F., Lenroot, R., Giedd, J., Bullmore, E.T., 2010. Disrupted modularity and local connectivity of brain functional networks in childhood-onset schizophrenia. In: Front. Syst. Neurosci., 4, p. 147. doi:10.3389/fnsys.2010.00147.

Alstott, J., Breakspear, M., Hagmann, P., Cammoun, L., Sporns, O., 2009. Modeling the impact of lesions in the human brain. PLoS Comput. Biol. 5 (6). doi:10.1371/journal.pcbi.1000408.

Behrens, T.E.J., Berg, H.J., Jbabdi, S., Rushworth, M.F.S., Woolrich, M.W., 2007. Probabilistic diffusion tractography with multiple fiber orientations: what can we gain? Neuroimage 34 (1), 144–155. doi:10.1016/j.neuroimage.2006.09.018.

Behrens, T.E.J., Woolrich, M.W., Jenkinson, M., Johansen-Berg, H., Nunes, R.G., Clare, S., Matthews, P.M., Brady, J.M., Smith, S.M., 2003. Characterization and propagation of uncertainty in diffusion-weighted MR imaging. Magn. Reson. Med. 50 (5), 1077–1088. doi:10.1002/mrm.10609.

Belyk, M., Brown, S., Lim, J., Kotz, S.A., 2017. Convergence of semantics and emotional expression within the IFG pars orbitalis. Neuroimage 156, 240–248. doi:10.1016/j.neuroimage.2017.04.020.

Benjamini, Y., Hochberg, Y., 1995. Controlling the false discovery rate: a practical and powerful approach to multiple testing. J. R. Stat. Soc. Ser. B 57, 289–300. doi:10.2307/2346101.

Benzi, M., Klymko, C., 2013. Total communicability as a centrality measure. J. Complex Netw. 1 (2), 124–149. doi:10.1093/comnet/cnt007.

Brandes, U., Fleischer, D., 2005. Centrality measures based on current flow. Lect. Notes Comput. Sci. 533–544. doi:10.1007/978-3-540-31856-9_44.

Brown, C.A., Johnson, N.F., Anderson-Mooney, A.J., Jicha, G.A., Shaw, L.M., Trojanowski, J.Q., Van Eldik, L.J., Schmitt, F.A., Smith, C.D., Gold, B.T., 2017. Development, validation and application of a new fornix template for studies of aging and preclinical Alzheimer's disease. NeuroImage Clin. 13, 106–115. doi:10.1016/j.nicl.2016.11.024.

Buchanan, C.R., Bastin, M.E., Ritchie, S.J., Liewald, D.C., Madole, J.W., Tucker-Drob, E.M., Deary, I.J., & Cox, S.R. (2020). The effect of network thresholding and weighting on structural brain networks in the UK Biobank. Neuroimage, 211(January), 116443. 10.1016/j.neuroimage.2019.116443

Cardinal, R.N., Parkinson, J.A., Hall, J., Everitt, B.J., 2002. Emotion and motivation: the role of the amygdala, ventral striatum, and prefrontal cortex. Neurosci. Biobehav. Rev. 26, 321–352. doi:10.1016/s0149-7634(02)00007-6.

Catani, M., Howard, R.J., Pajevic, S., Jones, D.K., 2002. Virtual *in vivo* interactive dissection of white matter fasciculi in the human brain. Neuroimage 17 (1), 77–94. doi:10.1006/nimg.2002.1136.

de Reus, M.A., van den Heuvel, M.P., 2013. Estimating false positives and negatives in brain networks. Neuroimage 70, 402–409. doi:10.1016/j.neuroimage.2012.12.066.

Donahue, C.J., Sotiropoulos, S.N., Jbabdi, S., Hernandez-Fernandez, M., Behrens, T.E., Dyrby, T.B., Coalson, T., Kennedy, H., Knoblauch, K., Van Essen, D.C., Glasser, M.F., 2016. Using diffusion tractography to predict cortical connection strength and distance: a quantitative comparison with tracers in the monkey. J. Neurosci. 36 (25), 6758–6770. doi:10.1523/JNEUROSCI.0493-16.2016.

Estrada, E., Hatano, N., 2008. Communicability in complex networks. Phys. Rev. D 77. doi:10.1103/PhysRevE.77.036111.

Estrada, E., Rodriguez-Velazquez, J.A., 2005. Subgraph centrality in complex networks. Phys. Rev. E 71 (5), 1–29. doi:10.1103/physreve.71.056103.

Evans, K.C., Wright, C.I., Wedig, M.M., Gold, A.L., Pollack, M.H., Rauch, S.L., 2008. A functional MRI study of amygdala responses to angry schematic faces in social anxiety disorder. Depress. Anxiety 25 (6), 496–505. doi:10.1002/da.20347.

Feinberg, D.A., Moeller, S., Smith, S.M., Auerbach, E., Ramanna, S., Glasser, M.F., Miller, K.L., Ugurbil, K., Yacoub, E., 2010. Multiplexed echo planar imaging for subsecond whole brain FMRI and fast diffusion imaging. PLoS ONE 5 (12), e15710. doi:10.1371/journal.pone.0015710.

Fischl, B., 2012. FreeSurfer. Neuroimage 62 (2), 774–781. doi:10.1016/j.neuroimage.2012.01.021.FreeSurfer.

Fischl, B., Salat, D.H., Busa, E., Albert, M., Dieterich, M., Haselgrove, C., Kouwe, A.Van Der, Killiany, R., Kennedy, D., Klaveness, S., Montillo, A., Makris, N., Rosen, B., Dale, A.M., 2002. Whole brain segmentation: automated labeling of neuroanatomical structures in the human brain. Neuron 33, 341–355. doi:10.1016/s0896-6273(02)00569-x.

Fornito, A., Zalesky, A., Bullmore, E., 2016. Fundamentals of Brain Network Analysis. Elsevier, pp. 383–419. doi:10.1016/B978-0-12-407908-3.00011-X Fundamentals of Brain Network Analysis.

Frank, D.W., Costa, V.D., Averbeck, B.B., Sabatinelli, D., 2019. Directional interconnectivity of the human amygdala, fusiform gyrus, and orbitofrontal cortex in emotional scene perception. J. Neurophysiol. 122 (4), 1530–1537. doi:10.1152/jn.00780.2018.

Glasser, M.F., Coalson, T.S., Robinson, E.C., Hacker, C.D., Harwell, J., Yacoub, E., Ugurbil, K., Andersson, J., Beckmann, C.F., Jenkinson, M., Smith, S.M., Van Essen, D.C., 2016. A multi-modal parcellation of human cerebral cortex. Nature 536 (7615), 171–178. doi:10.1038/nature18933.

Glasser, M.F., Sotiropoulos, S.N., Wilson, J.A., Coalson, T.S., Fischl, B., Andersson, J.L., Xu, J., Jbabdi, S., Webster, M., Polimeni, J.R., Van Essen, D.C., Jenkinson, M., 2013. The minimal preprocessing pipelines for the human connectome project. Neuroimage 80, 105–124. doi:10.1109/TMI.2012.2196707.

Goñi, J., Avena-Koenigsberger, A., Velez de Mendizabal, N., van den Heuvel, M.P., Betzel, R.F., Sporns, O., 2013. Exploring the morphospace of communication efficiency in complex networks. PLoS ONE 8 (3), e58070. doi:10.1371/journal.pone.0058070.

He, C., Gong, L., Yin, Y., Yuan, Y., Zhang, H., Lv, L., Zhang, X., Soares, J.C., Zhang, H., Xie, C., Zhang, Z., 2019. Amygdala connectivity mediates the association between anxiety and depression in patients with major depressive disorder. Brain Imaging Behav. 13 (4), 1146–1159. doi:10.1007/s11682-018-9923-z.

Hernandez-Fernandez, M., Reguly, I., Jbabdi, S., Giles, M., Smith, S., Sotiropoulos, S.N., 2019. Using GPUs to accelerate computational diffusion MRI: from microstructure estimation to tractography and connectomes. Neuroimage 188, 598–615. doi:10.1016/j.neuroimage.2018.12.015.

Horn, A., Ostwald, D., Reisert, M., Blankenburg, F., 2014. The structural-functional connectome and the default mode network of the human brain. Neuroimage 102, 142–151. doi:10.1016/j.neuroimage.2013.09.069.

Jbabdi, S., Johansen-Berg, H., 2011. Tractography: where do we go from here? Brain Connect. 1 (3), 169–183. doi:10.1089/brain.2011.0033.

Jbabdi, S., Sotiropoulos, S.N., Savio, A.M., Graña, M., Behrens, T.E.J., 2012. Model-based analysis of multishell diffusion MR data for tractography: how to get over fitting problems. Magn. Reson. Med. 68 (6), 1846–1855. doi:10.1002/mrm.24204.

Jenkinson, M., Beckmann, C.F., Behrens, T.E.J., Woolrich, M.W., Smith, S.M., 2012. FSL. Neuroimage 62 (2), 782–790. doi:10.1016/j.neuroimage.2011.09.015.

Kaiser, M., Martin, R., Andras, P., Young, M.P., 2007. Simulation of robustness against lesions of cortical networks. Eur. J. Neurosci. 25 (10), 3185–3192. doi:10.1111/j.1460-9568.2007.05574.x.

Kumar, V., Mang, S., Grodd, W., 2015. Direct diffusion-based parcellation of the human thalamus. Brain Struct. Funct. 220 (3), 1619–1635. doi:10.1007/s00429-014-0748-2.

Lang, P.J., Davis, M., 2006. Emotion, motivation, and the brain: reflex foundations in animal and human research. In: Progress in Brain Research, 156. Elsevier, pp. 3–29. doi:10.1016/S0079-6123(06)56001-7.

LeDoux, J., 2000. Emotion circuits in the brain. Annu. Rev. Neurosci. 23 (1), 155–184. doi:10.1176/foc.7.2.foc274.

Lindquist, K.A., Wager, T.D., Bliss-Moreau, E., Kober, H., Barrett, L.F., 2012. The brain basis of emotion: a meta-analytic review. Behav. Brain Sci. 35 (3), 121–143. doi:10.1017/S0140525x11000446.

Marcus, D.S., Harms, M.P., Snyder, A.Z., Jenkinson, M., Wilson, J.A., Glasser, M.F., Barch, D.M., Archie, K.A., Burgess, G.C., Ramaratnam, M., Hodge, M., Horton, W., Herrick, R., Olsen, T., McKay, M., House, M., Hileman, M., Reid, E., Harwell, J., Van Essen, D.C., 2013. Human connectome project informatics: quality control, database services, and data visualization. Neuroimage 80, 202–219. doi:10.1016/j.neuroimage.2013.05.077.

McDonald, A.J., 1998. Cortical pathways to the mammalian amygdala. Prog. Neurobiol. 55 (3), 257–332. doi:10.1016/S0301-0082(98)00003-3.

Moeller, S., Yacoub, E., Olman, C.A., Auerbach, E., Strupp, J., Harel, N., Uğurbil, K., 2010. Multiband multislice GE-EPI at 7 tesla, with 16-fold acceleration using partial parallel imaging with application to high spatial and temporal whole-brain fMRI. Magn. Reson. Med. 63 (5), 1144–1153. doi:10.1002/mrm.22361.

Morawetz, C., Bode, S., Baudewig, J., Heekeren, H.R., 2017a. Effective amygdala-prefrontal connectivity predicts individual differences in successful emotion regulation. Soc. Cogn. Affect. Neurosci. 12 (4), 569–585. doi:10.1093/scan/nsw169.

Morawetz, C., Bode, S., Derntl, B., Heekeren, H.R., 2017b. The effect of strategies, goals and stimulus material on the neural mechanisms of emotion regulation: a meta-analysis of fMRI studies. Neurosci. Biobehav. Rev. 72, 111–128. doi:10.1016/j.neubiorev.2016.11.014.

Newman, M.E.J., 2005. A measure of betweenness centrality based on random walks. Soc. Netw. 27 (1), 39–54. doi:10.1016/j.socnet.2004.11.009.

Owen, J.P., Wang, M.B., Mukherjee, P., 2016. Periventricular white matter is a nexus for network connectivity in the human brain. Brain Connect. 6 (7), 548–557. doi:10.1089/brain.2016.0431.

Pessoa, L., Adolphs, R., 2010. Emotion processing and the amygdala: from a “low road” to “many roads” of evaluating biological significance. Nat. Rev. Neurosci. 11 (11), 773–782. doi:10.1038/nrn2920.

Pestilli, F., Yeatman, J.D., Rokem, A., Kay, K.N., Wandell, B.A., 2014. Evaluation and statistical inference for human connectomes. Nat. Methods 11 (10), 1058–1063. doi:10.1038/nmeth.3098.

Phelps, E.A., Delgado, M.R., Nearing, K.I., LeDoux, J.E., 2004. Extinction learning in humans: role of the amygdala and vmPFC. Neuron 43 (6), 897–905. doi:10.1016/j.neuron.2004.08.042.

Ranganath, C., Ritchey, M., 2012. Two cortical systems for memory-guided behavior. Nat. Rev. Neurosci. 13 (10), 713–726. doi:10.1038/nrn3338.

Roine, T., Jeurissen, B., Perrone, D., Aelterman, J., Philips, W., Sijbers, J., Leemans, A., Roine, T., Perrone, D., 2019. Reproducibility and intercorrelation of graph theoretical measures in structural brain connectivity networks. Med. Image Anal. 52, 56–67. doi:10.1016/j.media.2018.10.009.

Rubinov, M., Sporns, O., 2010. Complex network measures of brain connectivity: uses and interpretations. Neuroimage 52 (3), 1059–1069. doi:10.1016/j.neuroimage.2009.10.003.

Schmitt, O., Eipert, P., Philipp, K., Kettlitz, R., Fuellen, G., Wree, A., 2012. The intrinsic connectome of the rat amygdala. Front. Neural Circuits 6, 81. doi:10.3389/fncir.2012.00081.

Setsompop, K., Gagoski, B.A., Polimeni, J.R., Witzel, T., Wedeen, V.J., Wald, L.L., 2012. Blipped-controlled aliasing in parallel imaging for simultaneous multislice echo planar imaging with reduced g-factor penalty. Magn. Reson. Med. 67 (5), 1210–1224. doi:10.1002/mrm.23097.

Sotiropoulos, S.N., Moeller, S., Jbabdi, S., Xu, J., Andersson, J.L., Auerbach, E.J., Yacoub, E., Feinberg, D., Setsompop, K., Wald, L.L., Behrens, T.E.J., Ugurbil, K., Lenglet, C., 2013. Effects of image reconstruction on fiber orientation mapping from multichannel diffusion MRI: reducing the noise floor using SENSE. Magn. Reson. Med. 70 (6), 1682–1689. doi:10.1002/mrm.24623.

Sotiropoulos, S.N., Zalesky, A., 2019. Building connectomes using diffusion MRI: why, how and but. NMR Biomed. 32, e3752. doi:10.1002/nbm.3752.

Spielberg, J.M., McGlinchey, R.E., Milberg, W.P., Salat, D.H., 2015. Brain network disturbance related to posttraumatic stress and traumatic brain injury in veterans. Biol. Psychiatry 78 (3), 210–216. doi:10.1016/j.biopsych.2015.02.013.

Sporns, O., 2013. Network attributes for segregation and integration in the human brain. Curr. Opin. Neurobiol. 23 (2), 162–171. doi:10.1016/j.conb.2012.11.015.

Stam, C.J., 2014. Modern network science of neurological disorders. Nat. Rev. Neurosci. 15 (10), 683–695. doi:10.1038/nrn3801.

Stefanacci, L., Suzuki, W.A., Amaral, D.G., 1996. Organization of connections between the amygdaloid complex and the perirhinal and parahippocampal cortices in macaque monkeys. J. Comp. Neurol. 375 (4), 552–582 10.1002/(SICI)1096-9861(19961125)375:4<552::AID–CNE2>3.0.CO;2-0.

Tamietto, M., De Gelder, B., 2010. Neural bases of the non-conscious perception of emotional signals. Nat. Rev. Neurosci. 11 (10), 697–709. doi:10.1038/nrn2889, Nature Publishing Group.

Tyll, S., Budinger, E., Noesselt, T., 2011. Thalamic influences on multisensory integration. Commun. Integr. Biol. 4 (4), 378–381. doi:10.4161/cib.4.4.15222.

Uğurbil, K., Xu, J., Auerbach, E.J., Moeller, S., Vu, A.T., Duarte-Carvajalino, J.M., Lenglet, C., Wu, X., Schmitter, S., Van de Moortele, P.F., Strupp, J., Sapiro, G., De Martino, F., Wang, D., Harel, N., Garwood, M., Chen, L., Feinberg, D.A., Smith, S.M., Yacoub, E., 2013. Pushing spatial and temporal resolution for functional and diffusion MRI in the human connectome project. Neuroimage 80, 80–104. doi:10.1016/j.neuroimage.2013.05.012.

van den Heuvel, M.P., de Reus, M.A., Feldman Barrett, L., Scholtens, L.H., Coopmans, F.M.T., Schmidt, R., Preuss, T.M., Rilling, J.K., Li, L., 2015. Comparison of diffusion tractography and tract-tracing measures of connectivity strength in rhesus macaque connectome. Hum. Brain Mapp. 36 (8), 3064–3075. doi:10.1002/hbm.22828.

Van Essen, D.C., Smith, S.M., Barch, D.M., Behrens, T.E.J., Yacoub, E., Ugurbil, K., 2013. The WU-Minn human connectome project: an overview. Neuroimage 80, 62–79. doi:10.1016/j.neuroimage.2013.05.041.

Vertes, R.P., Linley, S.B., Hoover, W.B., 2015. Limbic circuitry of the midline thalamus. Neurosci. Biobehav. Rev. 54, 89–107. doi:10.1016/j.neubiorev.2015.01.014.

Warrington, S., Bryant, K.L., Khrapitchev, A.A., Sallet, J., Charquero-Ballester, M., Douaud, G., Jbabdi, S., Mars, R.B., Sotiropoulos, S.N., 2020. XTRACT - standardized protocols for automated tractography in the human and macaque brain. Neuroimage 217, 116923. doi:10.1016/j.neuroimage.2020.116923.

Xu, Jie, Van Dam, N.T., Feng, C., Luo, Y., Ai, H., Gu, R., Xu, P., 2019. Anxious brain networks: a coordinate-based activation likelihood estimation meta-analysis of resting-state functional connectivity studies in anxiety. Neurosci. Biobehav. Rev. 96, 21–30. doi:10.1016/j.neubiorev.2018.11.005.

Xu, Junqian, Moeller, S., Strupp, J., Auerbach, E., Chen, L., Feinberg, D.A., Uğurbil, K., Yacoub, E., 2012. Highly accelerated whole brain imaging using aligned-blipped-controlled-aliasing multiband EPI. In: Proceedings of the International Society for Magnetic Resonance in Medicine, 20, p. 2306.

Zhang, M., Yang, F., Fan, F., Wang, Z., Hong, X., Tan, Y., Tan, S., Hong, L.E., 2020. Abnormal amygdala subregional-sensorimotor connectivity correlates with positive symptom in schizophrenia. NeuroImage Clin. 26, 102218. doi:10.1016/j.nicl.2020.102218.